ACS OMEGA

Article

Cite This: ACS Omega 2019, 4, 10322−10327

http://pubs.acs.org/journal/acsodf

Photostability of Monolayer Transition-Metal Dichalcogenides in Ambient Air and Acidic/Basic Aqueous Solutions

Wenjin Zhang, Kazunari Matsuda, and Yuhei Miyauchi*

Institute of Advanced Energy, Kyoto University, Uji, Kyoto 611-0011, Japan

Supporting Information

ABSTRACT: We report on the photostability of monolayer (1L) transition-metal dichalcogenides (TMDCs) in air and in aqueous solutions, as probed using photoluminescence spectroscopy. 1L-WSe_2 was readily degraded under continuous irradiation of visible light in aqueous solutions, whereas 1L-MoS_2 was relatively stable in both ambient air and aqueous solutions. The stability difference between these two materials was mainly ascribed to the oxidization reaction at the interface of 1L-TMDCs and the O_2/H_2O redox system induced by both band alignment and photogenerated holes. This interpretation was strongly supported by the observation of the lower degradation rate of 1L-WSe_2 in the dark and in degassed water with a lower concentration of dissolved oxygen compared with the degradation rate of 1L-WSe_2 in distilled water. Furthermore, the degradation rate was also nearly proportional to the number of photogenerated carriers. The degradation rate under acidic conditions was smaller than that under the basic conditions. The results are attributed to the oxidation/reduction potential of 1L-WSe_2 and to the dissolution reaction of degraded species, both of which are strongly pH-dependent.

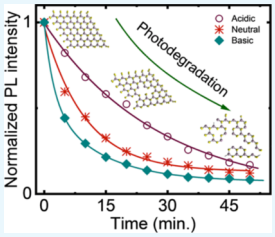

INTRODUCTION

Monolayers (1L) of transition-metal dichalcogenides (TMDCs) MX_2, where M is a transition metal (typically Mo or W) and X is a chalcogen (typically S, Se, or Te), have emerged as new direct-gap semiconductors with truly two-dimensional structures. Because of the striking change in their electronic structures from indirect (>2L) to direct band gap (1L) depending on their number of layers,[1−3] 1L-TMDCs show interesting optical and electrical properties which have strong potential for use in future electronic and optoelectronic devices such as phototransistors,[4−9] photodetectors,[10−12] light-emitting devices,[13,14] light modulators,[15] and solar cells.[16−18] Tunable photoluminescence (PL) has thus far been demonstrated using chemisorption and physisorption,[19−22] covalent bonding,[23,24] and electrostatic methods.[25,26] The electronic properties have also been studied using chemical doping and defect engineering.[27−29] Additionally, the applications of 1L-TMDCs as gas sensors or biosensors and photocatalysts for water splitting have been reported.[30−35] Electrochemical etching or oxidation reactions of atomically thin TMDCs under photoirradiation[36,37] or ozone exposure[38] conditions were also studied. These previous studies suggest that deep understanding of the influence of surface reactions on the physical properties and stability of 1L-TMDCs is important for realizing their application in various environments such as ambient air or wet conditions. However, knowledge of the stability of 1L-TMDCs under such conditions is limited.

In this paper, we report on the stability of the most typical 1L-TMDCs—1L-WSe_2 and 1L-MoS_2—in ambient air and acidic/basic aqueous solutions under visible-light irradiation. The PL intensities of 1L-WSe_2 distinctly decreased in acidic/basic aqueous solutions, whereas MoS_2 was stable under the same conditions and its PL intensity showed a negligible decrease. The PL spectral shape did not show a remarkable change with increasing irradiation time for either 1L-WSe_2 or 1L-MoS_2, suggesting that the change in the PL intensity was not caused by photoinduced carrier doping but was mainly attributable to photoinduced degradation. We confirmed that the degradation rate was lower in the dark and in degassed water than in distilled water, suggesting that both light and dissolved oxygen are necessary for photodegradation reactions. Furthermore, 1L-WSe_2 under acidic and neutral conditions showed a more moderate degradation rate than that under the basic condition. These results suggest that the electrochemical reaction with 1L-TMDCs and photogenerated holes in the presence of oxygen and water is the key mechanism of the degradation. This mechanism is effective for 1L-WSe_2 and ineffective for MoS_2 because of the difference in the relative alignment among the oxidation/reduction potentials of O_2/H_2O and the levels of the valence and conduction bands of each 1L-TMDC.

RESULTS AND DISCUSSION

Figure 1 shows the schematic of the optical system for the PL measurements in air or aqueous solutions. 1L-TMDCs prepared on a transparent glass substrate (Figure S1) were irradiated with visible wavelength light (580 nm) with a constant power density (800 W cm^{-2}). The signal was recorded using a silicon charge-coupled device (CCD) detector equipped with a spectrometer (see the Experimental Methods section for details).

Received: April 15, 2019
Accepted: May 31, 2019
Published: June 13, 2019

DOI: 10.1021/acsomega.9b01067
ACS Omega 2019, 4, 10322−10327

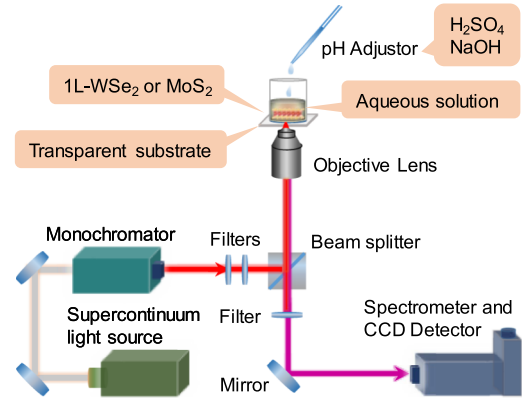

Figure 1. Schematic of the optical system for the PL measurement. White light from a supercontinuum light source is separated using a monochromator and optical filters, and only visible light with selected wavelength is focused on to the sample on a glass substrate. The samples were placed in air or in aqueous solution during the measurement.

Figure 2a,b shows the PL intensity and the normalized PL spectra of 1L-WSe_2 under ambient air at different photo-

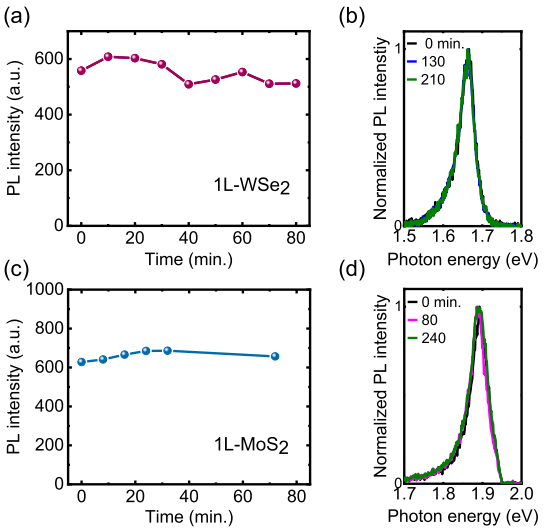

Figure 2. Time-dependent PL intensity (a,c) and normalized PL spectra (b,d) in ambient air. (a,b) are for 1L-WSe_2 and (c,d) are for 1L-MoS_2.

irradiation times. As shown in Figure 2a, the PL intensity decreased slightly within 90 min under photoirradiation (580 nm, 800 W cm^{-2}, which is in the linear region shown in Figure S2). By contrast, 1L-MoS_2 showed a negligible change in PL intensity (Figure 2c). The normalized PL spectra show an undetectable shape change in the spectra of both 1L-WSe_2 and 1L-MoS_2 (Figure 2b,d). Because the optical absorption coefficients of 1L-TMDCs at 580 nm are similar (1×10^5 to 2×10^5 cm^{-1}),[39,40] we expected similar numbers of electrons and holes to be photogenerated in these samples. Thus, these results imply that the stability of 1L-WSe_2 is slightly lower than that of MoS_2 in ambient air under photoirradiation.

Because the properties of 1L-TMDCs are known to be strongly modified by electrochemical effects at the surfaces,[22,41] we next studied their stabilities in water under light irradiation. Under these conditions, water molecules are adsorbed onto the surface and electrochemical effects because the oxygen/water redox couple becomes important.[41] We first performed PL measurements with the 1L-TMDCs in distilled water and then with the 1L-TMDCs in acidic/basic solutions. As shown in Figure 3a,c, the PL intensity of 1L-WSe_2 (Figure 3a) in aqueous solution rapidly decreased with increasing irradiation time, whereas the PL intensity of 1L-MoS_2 (Figure 3c) was stable under all of the investigated conditions. The main decrease of the 1L-WSe_2 PL intensity under neutral (distilled water) and basic conditions occurred within the first 10−15 min; the decrease then slowed, likely because of the increased concentration of the degradation products from 1L-WSe_2. Under the acidic condition, as shown in Figure 3a, 1L-WSe_2 exhibited a relatively moderate degradation rate, in contrast to the fast degradation observed under other conditions. The original PL intensities decreased by approximately 15, 40, and 55% within 10 min in acidic (pH = 2), neutral (pH = 7), and basic (pH = 12) conditions, respectively. The normalized PL spectra of 1L-WSe_2 and 1L-MoS_2 show almost no change of the spectral shape within the irradiation time as shown in Figure 3b,d. We also confirmed the photo-induced degradation of 1L-WSe_2 in water directly by observing optical and PL images before and after the photoirradiation (Figure S3).

To elucidate the mechanism of the material-dependent degradation behavior and the differences among degradation rates of the materials in different environments, we consider O_2/H_2O redox couple and the electrochemical reaction at the interface between aqueous solutions and 1L-TMDCs. The effects of O_2 and H_2O molecules on the optical and electrical properties of the 1L-TMDCs were reported.[22,41] The transfer of photogenerated electrons or holes may be a main factor related to the degradation or decomposition of the 1L-TMDCs in an O_2/H_2O system, depending on the band alignment of the semiconductors with the oxidation/reduction potentials of O_2/H_2O. In general, photogenerated holes (h^+) can facilitate the oxidation of compound semiconductors (AB)[42] and destruct their original structures

$$AB + zh^+ + solv \rightarrow A\,(oxidation) + B^{z+}\bullet solv \quad (1)$$

where z represents the number of holes and solv is solvent. In the current study, A and B are the transition metal and chalcogen that compose the semiconductors, respectively.

The band alignment of 1L-WSe_2 relative to vacuum is shown in Figure 4a. The conduction-band minimum is near −3.6 eV, which is much higher than the H^+/H_2 reduction potential (ca. −4.83 eV).[43−47] Thus, some of the photogenerated electrons can reduce H^+ to H_2. This process can also occur for 1L-MoS_2 (Figure 4b), which has a conduction-band minimum at approximately −4.1 eV;[47,48] however, the smaller energy difference from $\phi(H^+/H_2)$ results in a lower electron driving force/rate to reduce H^+ to H_2 in comparison with 1L-WSe_2, as reported in previous studies.[49,50] The valance-band edge of 1L-WSe_2 is at approximately −5.2 eV,[47,51] which is higher than the O_2/H_2O potential (ca. −5.66 eV). Photogenerated holes in WSe_2 cannot totally recombine with the photogenerated electrons because some of the electrons have already been used to reduce H^+ to H_2. Thus, the excess amount of holes degrades the 1L-WSe_2 itself rather than oxygenating H_2O[42,52] that is energetically unfavorable. These processes are expressed in eqs 2 and 3[36,53,54]

$$2H^+ + 2e^- \rightarrow H_2 \quad (2)$$

DOI: 10.1021/acsomega.9b01067
ACS Omega 2019, 4, 10322−10327

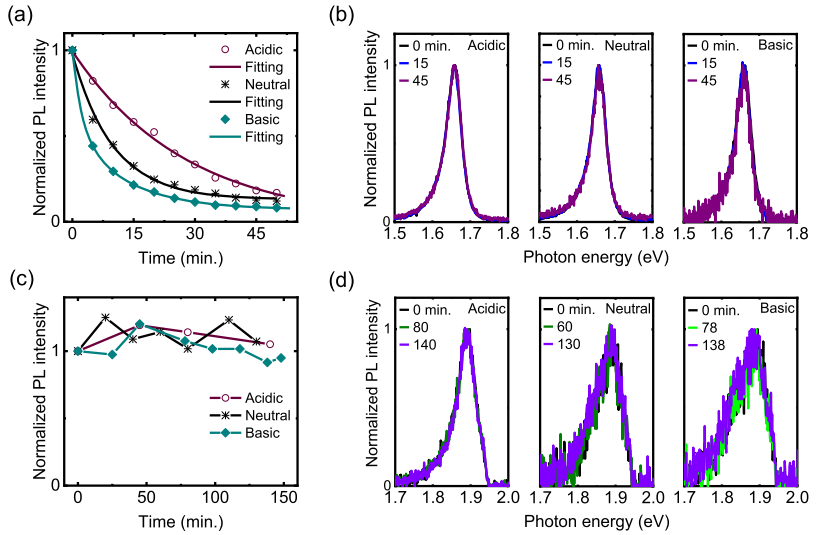

Figure 3. Time-dependent PL intensity and the spectral shape of (a,b) 1L-WSe_2 and (c,d) 1L-MoS_2 under acidic, neutral, and basic conditions. The solid curves in (a) are the results of fitting using single- or double-exponential functions.

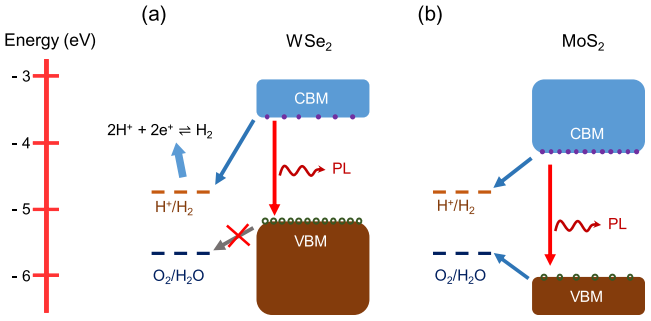

Figure 4. Band alignment of (a) 1L-WSe_2 and (b) 1L-MoS_2 with the water redox potential.

$$2WSe_2 + 8h^+ + 8H_2O + 7O_2 \rightleftharpoons 2WO_3 + 4SeO_4^{2-} + 16H^+ \quad (3)$$

For 1L-MoS_2, the valence-band maximum is at approximately −6.0 eV which is lower than the potential of O_2/H_2O and some of the photogenerated holes may oxygenate H_2O to O_2. In this case, fewer excess holes remain and MoS_2 itself is not likely to be degraded within a short time. Thus, we can explain the difference in the degradation behaviors between 1L-MoS_2 and 1L-WSe_2. Specifically, the change in pH results in a change of the redox potentials of the O_2/H_2O couple tested in this study (from −5.54 to −4.95 eV) between pH 2 and 12, and the oxidation and reduction potentials for 1L-WSe_2 are also shifted.[42] When H^+ (or OH^-) is directly involved in the oxidization/reduction reaction, as in eq 3, the relative potentials between O_2/H_2O and 1L-WSe_2 will change,[42] becoming one of the factors influencing the pH-dependent degradation effect.

Furthermore, WO_3 will be involved in a more complicated pH-dependent reaction in aqueous solution because of its thermodynamic instability.[54,55] To further understand the pH dependence, we also consider the second reaction of the oxidation product

$$WO_3 + H_2O \rightleftharpoons WO_4^{2-} + 2H^+ \quad (4)$$

whose reaction rate also strongly depends on the solution pH. According to eqs 3 and 4, the pH dependence of the photodegradation rate can be understood as follows: under the basic condition, the reaction resulting in the dissolution of WO_3 should become faster than that under the acidic condition. Thus, the fast degradation under the basic condition is attributable to both the enhanced oxidation reaction and the dissolution reaction of WSe_2 and WO_3, which generate more defects and edges[56−59] in the 1L-WSe_2 flake. This hypothesis is supported by the pH dependence of the decrease of the PL intensities (Figure 3). For the PL intensity under the acidic condition, the time trace is well fitted by a single-exponential function. By contrast, the trace corresponding to the basic condition shows a much faster initial degradation that cannot be explained by a single reaction, implying involvement of an additional electrochemical process with a different time scale, as expressed in eq 4. WSe_2 degradation species differ among the acidic (WO_3 and SeO_4^{2-}), neutral, and basic conditions (WO_4^{2-} and SeO_4^{2-}).[60] This observation is consistent with the recently reported pH-dependent Gibbs free energy of WSe_2.[60] For samples under acidic conditions, we can simply set the degradation rate equation as $dA/dt = -\alpha A$, where A is the undegraded area of 1L-WSe_2 at time t and α is the rate constant. Solving this equation gives $A = A_0\, e^{-\alpha t}$, where A_0 is the original area of 1L-WSe_2. The undegraded area of 1L-WSe_2 decreases exponentially, and the decrease in PL intensity can be well reproduced using a single-exponential function, as shown in Figure 3.

To further confirm the photoinduced degradation effects, we measured the PL properties of the samples kept in the dark and in degassed water. The samples kept under dark conditions were not illuminated except during the measurements. As shown in Figure 5, the degradation reactions of 1L-WSe_2 in both dark (not degassed) (~46%) and degassed (with light) conditions (~38%) for 30 min are much slower than that of 1L-WSe_2 in distilled water (not degassed, with light) (~82%), which supports our hypothesis that the degradation is mainly induced by the electrochemical effects of the photogenerated holes and dissolved oxygen in water.[61,62]

The effect of photogenerated carrier density on the degradation rate was also confirmed. As shown in Figure 6,

DOI: 10.1021/acsomega.9b01067
ACS Omega 2019, 4, 10322−10327

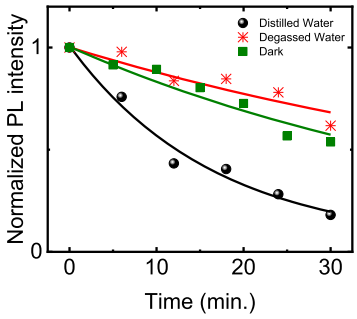

Figure 5. Time-dependent PL intensity of 1L-WSe_2 in distilled water, water in the absence of light (dark) and degassed water. The solid curves are the results of fitting using single-exponential functions.

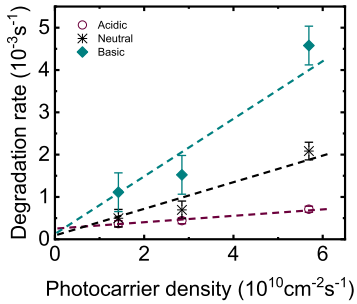

Figure 6. Photocarrier-density-dependent degradation rate in acidic, neutral, and basic conditions. The dashed lines are the results of fitting.

the degradation rates of 1L-WSe_2 under all conditions (acidic, neutral, and basic) are nearly proportional to the density of photogenerated electrons/holes, which strongly supports the hypothesis that degradation occurs mainly from photoinduced effects. The wavelength-dependent degradation rate, as shown in Figure S4, further supports this hypothesis. Moreover, under the acidic condition, the degradation rate was almost one order of magnitude smaller than that under the basic condition, which also supports the aforementioned hypothesis. By extrapolation, the degradation rate is between 0.1×10^{-3} and 0.3×10^{-3} s^{-1} when the photocarrier density is 0 (Figure 6), consistent with the degradation rate in the dark (Figure 5), where a slow degradation with a rate of $\sim 0.3 \times 10^{-3}$ s^{-1} is observed.

CONCLUSIONS

In summary, we studied the stability of 1L-WSe_2 and 1L-MoS_2 in ambient air, distilled water, and acidic/basic aqueous solutions under light irradiation. In contrast to the good stability of both materials in ambient air, 1L-MoS_2 was found to be much more stable than 1L-WSe_2 under aqueous conditions. These results were consistently attributed to electrochemical reactions involving photoinduced electrons/holes at the interface of 1L-WSe_2 and the O_2/H_2O redox system. A much lower degradation rate was observed for 1L-WSe_2 under acidic conditions than under basic conditions, which we attributed mainly to the pH dependence of the oxidation/reduction potential of WSe_2 and to the further reaction of the oxidation species. We also confirmed that the degradation rates of 1L-WSe_2 in both degassed water and dark conditions are much lower than those of 1L-WSe_2 in distilled water. The slower degradation in degassed water and dark conditions supports our hypothesis that photoinduced electrons/holes and dissolved oxygen are the main contributors to the degradation of 1L-WSe_2. Our results may provide insights into the effects of photogenerated electrons/holes and electrochemical phenomena at the interface of atomically thin semiconductors and an O_2/H_2O redox system on their stability, which is important for their applications in realistic environments because these effects are unavoidable when a monolayer material with a large specific surface area is in a practical environment with finite humidity or in solution.

EXPERIMENTAL METHODS

1L-TMDC samples were prepared from a bulk single crystal (hq graphene) using a standard mechanical exfoliation method. The thickness of an exfoliated TMDC was first determined via image contrast using an optical microscope, and the Raman and PL spectra were then used to confirm the thickness. The exfoliated 1L-TMDCs were transferred onto a transparent glass substrate using polydimethylsiloxane, and the substrate with 1L-TMDCs was then tightly bound with a glass tube to compose a liquid reservoir in which sufficient liquid could be kept over the sample for the optical measurements in aqueous solutions. H_2SO_4 and NaOH were used as the pH adjustors to attain acidic, neutral, or basic aqueous solutions. Degassed water was prepared using argon gas bubbling to reduce the dissolved oxygen concentration.

Optical measurements were performed through the transparent glass substrate using a homemade optical measurement system with a supercontinuum light source (20 ps pulse duration and 40 MHz frequency) equipped with a monochromator (Figure 1). PL spectra were recorded with the samples in ambient air, in water, and finally in acidic and basic aqueous solutions using a liquid nitrogen-cooled silicon CCD detector. The measurements were performed at regular intervals (5 min) with a signal acquisition time of 5 s. During the measurements, samples were kept illuminated by light with a power density of 800 W cm^{-2}, which is in the linear region as shown in Figure S2, except for the experiment under dark conditions. The amount of water and aqueous solutions was kept the same, and all the measurements were performed at room temperature.

ASSOCIATED CONTENT

Supporting Information

The Supporting Information is available free of charge on the ACS Publications website at DOI: 10.1021/acsomega.9b01067.

Fundamental Raman and PL spectra of 1L-WSe_2 and 1L-MoS_2 used in this study; excitation power dependence of PL intensity of 1L-WSe_2 and the wavelength dependence of the degradation rate in the distilled water condition; optical and PL images of 1L-WSe_2 before and after photoirradiation (PDF)

AUTHOR INFORMATION

Corresponding Author

*E-mail: miyauchi@iae.kyoto-u.ac.jp.

ORCID

Kazunari Matsuda: 0000-0002-3990-8484

Yuhei Miyauchi: 0000-0002-0945-0265

Notes

The authors declare no competing financial interest.

DOI: 10.1021/acsomega.9b01067
ACS Omega 2019, 4, 10322−10327

■ ACKNOWLEDGMENTS

This research was supported by JSPS KAKENHI grant numbers JP16H00911, JP15K13337, JP15H05408, JP15K13500, JP16H00910, JP16H06331, JP17K19055, by the Asahi Glass Foundation, by JST CREST (JPMJCR16F3, JPMJCR18I5), by the Research Foundation for Opto-Science and Technology, and by the Nakatani Foundation.

■ REFERENCES

(1) Mak, K. F.; Lee, C.; Hone, J.; Shan, J.; Heinz, T. Atomically Thin MoS_2: A New Direct-Gap Semiconductor. *Phys. Rev. Lett.* **2010**, *105*, 136805.
(2) Yu, H.; Cui, X.; Xu, X.; Yao, W. Valley Excitons in Two-Dimensional Semiconductors. *Nat. Sci. Rev.* **2015**, *2*, 57−70.
(3) Kang, J.; Zhang, L.; Wei, S.-H. A Unified Understanding of the Thickness-Dependent Bandgap Transition in Hexagonal Two-Dimensional Semiconductors. *J. Phys. Chem. Lett.* **2016**, *7*, 597−602.
(4) Nouchi, R.; Tanigaki, K. Charge-Density Depinning at Metal Contacts of Graphene Field-Effect Transistors. *Appl. Phys. Lett.* **2010**, *96*, 253503.
(5) Yin, Z.; Li, H.; Li, H.; Jiang, L.; Shi, Y.; Sun, Y.; Lu, G.; Zhang, Q.; Chen, X.; Zhang, H. Single-Layer MoS_2 Phototransistors. *ACS Nano* **2012**, *6*, 74−80.
(6) Liu, W.; Kang, J.; Sarkar, D.; Khatami, Y.; Jena, D.; Banerjee, K. Role of Metal Contacts in Designing High-Performance Monolayer n-Type WSe_2 Field Effect Transistors. *Nano Lett.* **2013**, *13*, 1983−1990.
(7) Wu, C.-C.; Jariwala, D.; Sangwan, V. K.; Marks, T. J.; Hersam, M. C.; Lauhon, L. J. Elucidating the Photoresponse of Ultrathin MoS_2 Field-Effect Transistors by Scanning Photocurrent Microscopy. *J. Phys. Chem. Lett.* **2013**, *4*, 2508−2513.
(8) Gao, Y.; Liu, Z.; Sun, D.-M.; Huang, L.; Ma, L.-P.; Yin, L.-C.; Ma, T.; Zhang, Z.; Ma, X.-L.; Peng, L.-M.; et al. Large-Area Synthesis of High-Quality and Uniform Monolayer WS_2 on Reusable Au Foils. *Nat. Commun.* **2015**, *6*, 8569.
(9) Kretschmer, S.; Komsa, H.-P.; Bøggild, P.; Krasheninnikov, A. V. Structural Transformations in Two-Dimensional Transition-Metal Dichalcogenide MoS_2 Under Electron Beam: Insights from First-Principles Calculations. *J. Phys. Chem. Lett.* **2017**, *8*, 3061−3067.
(10) Lopez-Sanchez, O.; Lembke, D.; Kayci, M.; Radenovic, A.; Kis, A. Ultrasensitive Photodetectors Based on Monolayer MoS_2. *Nat. Nanotechnol.* **2013**, *8*, 497−501.
(11) Tan, D.; Lim, H. E.; Wang, F.; Mohamed, N. B.; Mouri, S.; Zhang, W.; Miyauchi, Y.; Ohfuchi, M.; Matsuda, K. Anisotropic Optical and Electronic Properties of Two-Dimensional Layered Germanium Sulfide. *Nano Res.* **2017**, *10*, 546−555.
(12) Yu, W.; Li, S.; Zhang, Y.; Ma, W.; Sun, T.; Yuan, J.; Fu, K.; Bao, Q. Near-Infrared Photodetectors Based on $MoTe_2$/Graphene Heterostructure with High Responsivity and Flexibility. *Small* **2017**, *13*, 1700268.
(13) Sundaram, R. S.; Engel, M.; Lombardo, A.; Krupke, R.; Ferrari, A. C.; Avouris, P.; Steiner, M. Electroluminescence in Single Layer MoS_2. *Nano Lett.* **2013**, *13*, 1416−1421.
(14) Ross, J. S.; Klement, P.; Jones, A. M.; Ghimire, N. J.; Yan, J.; Mandrus, D. G.; Taniguchi, T.; Watanabe, K.; Kitamura, K.; Yao, W.; et al. Electrically Tunable Excitonic Light-Emitting Diodes Based on Monolayer WSe_2 p-n Junctions. *Nat. Nanotechnol.* **2014**, *9*, 268−272.
(15) Tongay, S.; Zhou, J.; Ataca, C.; Liu, J.; Kang, J. S.; Matthews, T. S.; You, L.; Li, J.; Grossman, J. C.; Wu, J. Broad-Range Modulation of Light Emission in Two-Dimensional Semiconductors by Molecular Physisorption Gating. *Nano Lett.* **2013**, *13*, 2831−2836.
(16) Bernardi, M.; Palummo, M.; Grossman, J. C. Extraordinary Sunlight Absorption and One Nanometer Thick Photovoltaics Using Two-Dimensional Monolayer Materials. *Nano Lett.* **2013**, *13*, 3664−3670.
(17) Tsuboi, Y.; Wang, F.; Kozawa, D.; Funahashi, K.; Mouri, S.; Miyauchi, Y.; Takenobu, T.; Matsuda, K. Enhanced Photovoltaic Performances of Graphene/Si Solar Cells by Insertion of a MoS_2 Thin Film. *Nanoscale* **2015**, *7*, 14476−14482.
(18) Zhou, Y.; Xu, W.; Sheng, Y.; Huang, H.; Zhang, Q.; Hou, L.; Shautsova, V.; Warner, J. H. Symmetry-Controlled Reversible Photovoltaic Current Flow in Ultrathin All 2D Vertically Stacked Graphene/MoS_2/WS_2/Graphene Devices. *ACS Appl. Mater. Interfaces* **2019**, *11*, 2234−2242.
(19) Mouri, S.; Miyauchi, Y.; Matsuda, K. Tunable Photoluminescence of Monolayer MoS_2 via Chemical Doping. *Nano Lett.* **2013**, *13*, 5944−5948.
(20) Dhakal, K. P.; Duong, D. L.; Lee, J.; Nam, H.; Kim, M.; Kan, M.; Lee, Y. H.; Kim, J. Confocal Absorption Spectral Imaging of MoS_2: Optical Transitions Depending on the Atomic Thickness of Intrinsic and Chemically Doped MoS_2. *Nanoscale* **2014**, *6*, 13028−13035.
(21) Kiriya, D.; Tosun, M.; Zhao, P.; Kang, J. S.; Javey, A. Air-Stable Surface Charge Transfer Doping of MoS_2 by Benzyl Viologen. *J. Am. Chem. Soc.* **2014**, *136*, 7853−7856.
(22) Wang, S.; Zhao, W.; Giustiniano, F.; Eda, G. Effect of Oxygen and Ozone on P-Type Doping of Ultra-Thin WSe_2 and $MoSe_2$ Field Effect Transistors. *Phys. Chem. Chem. Phys.* **2016**, *18*, 4304−4309.
(23) Suh, J.; Park, T.-E.; Lin, D.-Y.; Fu, D.; Park, J.; Jung, H. J.; Chen, Y.; Ko, C.; Jang, C.; Sun, Y.; et al. Doping against the Native Propensity of MoS_2: Degenerate Hole Doping by Cation Substitution. *Nano Lett.* **2014**, *14*, 6976−6982.
(24) Nan, H.; Wang, Z.; Wang, W.; Liang, Z.; Lu, Y.; Chen, Q.; He, D.; Tan, P.; Miao, F.; Wang, X.; et al. Strong Photoluminescence Enhancement of MoS_2 through Defect Engineering and Oxygen Bonding. *ACS Nano* **2014**, *8*, 5738−5745.
(25) Mak, K. F.; He, K.; Lee, C.; Lee, G. H.; Hone, J.; Heinz, T. F.; Shan, J. Tightly Bound Trions in Monolayer MoS_2. *Nat. Mater.* **2013**, *12*, 207−211.
(26) Atallah, T. L.; Wang, J.; Bosch, M.; Seo, D.; Burke, R. A.; Moneer, O.; Zhu, J.; Theibault, M.; Brus, L. E.; Hone, J.; et al. Electrostatic Screening of Charged Defects in Monolayer MoS_2. *J. Phys. Chem. Lett.* **2017**, *8*, 2148−2152.
(27) Liu, B.; Chen, L.; Liu, G.; Abbas, A. N.; Fathi, M.; Zhou, C. High-Performance Chemical Sensing Using Schottky-Contacted Chemical Vapor Deposition Grown Monolayer MoS_2 Transistors. *ACS Nano* **2014**, *8*, 5304−5314.
(28) Bertolazzi, S.; Bonacchi, S.; Nan, G.; Pershin, A.; Beljonne, D.; Samorì, P. Engineering Chemically Active Defects in Monolayer MoS_2 Transistors via Ion-Beam Irradiation and Their Healing via Vapor Deposition of Alkanethiols. *Adv. Mater.* **2017**, *29*, 1606760.
(29) Neupane, G. P.; Tran, M. D.; Yun, S. J.; Kim, H.; Seo, C.; Lee, J.; Han, G. H.; Sood, A. K.; Kim, J. Simple Chemical Treatment to N-Dope Transition-Metal Dichalcogenides and Enhance the Optical and Electrical Characteristics. *ACS Appl. Mater. Interfaces* **2017**, *9*, 11950−11958.
(30) Voiry, D.; Yamaguchi, H.; Li, J.; Silva, R.; Alves, D. C. B.; Fujita, T.; Chen, M.; Asefa, T.; Shenoy, V. B.; Eda, G.; et al. Enhanced Catalytic Activity in Strained Chemically Exfoliated WS_2 Nanosheets for Hydrogen Evolution. *Nat. Mater.* **2013**, *12*, 850−855.
(31) Zhuang, H. L.; Hennig, R. G. Single-Layer Group-III Monochalcogenide Photocatalysts for Water Splitting. *Chem. Mater.* **2013**, *25*, 3232−3238.
(32) Late, D. J.; Huang, Y.-K.; Liu, B.; Acharya, J.; Shirodkar, S. N.; Luo, J.; Yan, A.; Charles, D.; Waghmare, U. V.; Dravid, V. P.; et al. Sensing Behavior of Atomically Thin-Layered MoS_2 Transistors. *ACS Nano* **2013**, *7*, 4879−4891.
(33) Lee, J.; Dak, P.; Lee, Y.; Park, H.; Choi, W.; Alam, M. A.; Kim, S. Two-Dimensional Layered MoS_2 Biosensors Enable Highly Sensitive Detection of Biomolecules. *Sci. Rep.* **2014**, *4*, 7352.
(34) Rao, C. N. R.; Gopalakrishnan, K.; Maitra, U. Comparative Study of Potential Applications of Graphene, MoS_2, and Other Two-Dimensional Materials in Energy Devices, Sensors, and Related Areas. *ACS Appl. Mater. Interfaces* **2015**, *7*, 7809−7832.
(35) Ko, K. Y.; Park, K.; Lee, S.; Kim, Y.; Woo, W. J.; Kim, D.; Song, J.-G.; Park, J.; Kim, H. Recovery Improvement for Large-Area Tungsten Diselenide Gas Sensors. *ACS Appl. Mater. Interfaces* **2018**, *10*, 23910−23917.

DOI: 10.1021/acsomega.9b01067
ACS Omega 2019, 4, 10322−10327

(36) Sunamura, K.; Page, T. R.; Yoshida, K.; Yano, T.-a.; Hayamizu, Y. Laser-Induced Electrochemical Thinning of MoS_2. *J. Mater. Chem. C* **2016**, *4*, 3268−3273.
(37) Oh, H. M.; Han, G. H.; Kim, H.; Bae, J. J.; Jeong, M. S.; Lee, Y. H. Photochemical Reaction in Monolayer MoS_2 via Correlated Photoluminescence, Raman Spectroscopy, and Atomic Force Microscopy. *ACS Nano* **2016**, *10*, 5230−5236.
(38) Yamamoto, M.; Dutta, S.; Aikawa, S.; Nakaharai, S.; Wakabayashi, K.; Fuhrer, M. S.; Ueno, K.; Tsukagoshi, K. Self-Limiting Layer-by-Layer Oxidation of Atomically Thin WSe_2. *Nano Lett.* **2015**, *15*, 2067−2073.
(39) Liu, H.-L.; Shen, C.-C.; Su, S.-H.; Hsu, C.-L.; Li, M.-Y.; Li, L.-J. Optical Properties of Monolayer Transition Metal Dichalcogenides Probed by Spectroscopic Ellipsometry. *Appl. Phys. Lett.* **2014**, *105*, 201905.
(40) Arora, A.; Koperski, M.; Nogajewski, K.; Marcus, J.; Faugeras, C.; Potemski, M. Excitonic Resonances in Thin Films of WSe_2: From Monolayer to Bulk Material. *Nanoscale* **2015**, *7*, 10421−10429.
(41) Zhang, W.; Matsuda, K.; Miyauchi, Y. PH-Dependent Photoluminescence Properties of Monolayer Transition-Metal Dichalcogenides Immersed in an Aqueous Solution. *J. Phys. Chem. C* **2018**, *122*, 13175−13181.
(42) Chen, S.; Wang, L.-W. Thermodynamic Oxidation and Reduction Potentials of Photocatalytic Semiconductors in Aqueous Solution. *Chem. Mater.* **2012**, *24*, 3659−3666.
(43) Chakrapani, V.; Angus, J. C.; Anderson, A. B.; Wolter, S. D.; Stoner, B. R.; Sumanasekera, G. U. Charge Transfer Equilibria Between Diamond and an Aqueous Oxygen Electrochemical Redox Couple. *Science* **2007**, *318*, 1424−1430.
(44) Aguirre, C. M.; Levesque, P. L.; Paillet, M.; Lapointe, F.; St-Antoine, B. C.; Desjardins, P.; Martel, R. The Role of the Oxygen/Water Redox Couple in Suppressing Electron Conduction in Field-Effect Transistors. *Adv. Mater.* **2009**, *21*, 3087−3091.
(45) Wang, F.; Shifa, T. A.; Zhan, X.; Huang, Y.; Liu, K.; Cheng, Z.; Jiang, C.; He, J. Recent Advances in Transition-Metal Dichalcogenide Based Nanomaterials for Water Splitting. *Nanoscale* **2015**, *7*, 19764−19788.
(46) Liu, Y.; Stradins, P.; Wei, S.-H. Van Der Waals Metal-Semiconductor Junction: Weak Fermi Level Pinning Enables Effective Tuning of Schottky Barrier. *Sci. Adv.* **2016**, *2*, No. e1600069.
(47) Zhang, C.; Gong, C.; Nie, Y.; Min, K.-A.; Liang, C.; Oh, Y. J.; Zhang, H.; Wang, W.; Hong, S.; Colombo, L.; et al. Systematic Study of Electronic Structure and Band Alignment of Monolayer Transition Metal Dichalcogenides in Van Der Waals Heterostructures. *2D Mater.* **2016**, *4*, 015026.
(48) Choudhury, P.; Ravavarapu, L.; Dekle, R.; Chowdhury, S. Modulating Electronic and Optical Properties of Monolayer MoS_2 Using Nonbonded Phthalocyanine Molecules. *J. Phys. Chem. C* **2017**, *121*, 2959−2967.
(49) Jaramillo, T. F.; Jørgensen, K. P.; Bonde, J.; Nielsen, J. H.; Horch, S.; Chorkendorff, I. Identification of Active Edge Sites for Electrochemical H_2 Evolution from MoS_2 Nanocatalysts. *Science* **2007**, *317*, 100−102.
(50) Joshi, R. K.; Shukla, S.; Saxena, S.; Lee, G.-H.; Sahajwalla, V.; Alwarappan, S. Hydrogen Generation via Photoelectrochemical Water Splitting Using Chemically Exfoliated MoS_2 Layers. *AIP Adv* **2016**, *6*, 015315.
(51) Rasmussen, F. A.; Thygesen, K. S. Computational 2D Materials Database: Electronic Structure of Transition-Metal Dichalcogenides and Oxides. *J. Phys. Chem. C* **2015**, *119*, 13169−13183.
(52) Fujii, K. In *Photoelectrochemical Solar Fuel Production*, 1st ed.; Giménez, S., Bisquert, J., Eds.; Springer International Publishing, 2016.
(53) Böhmisch, M.; Burmeister, F.; Boneberg, J.; Leiderer, P. Nanostructuring on WSe_2 with the Atomic Force Microscope by a Potential Controlled Electrochemical Reaction. *Appl. Phys. Lett.* **1996**, *69*, 1882−1884.
(54) Huang, Y.-T.; Dodda, A.; Schulman, D. S.; Sebastian, A.; Zhang, F.; Buzzell, D.; Terrones, M.; Feng, S.-P.; Das, S. Anomalous Corrosion of Bulk Transition Metal Diselenides Leading to Stable Monolayers. *ACS Appl. Mater. Interfaces* **2017**, *9*, 39059−39068.
(55) Eng, A. Y. S.; Ambrosi, A.; Sofer, Z.; Šimek, P.; Pumera, M. Electrochemistry of Transition Metal Dichalcogenides: Strong Dependence on the Metal-to-Chalcogen Composition and Exfoliation Method. *ACS Nano* **2014**, *8*, 12185−12198.
(56) Liu, X.; Xu, T.; Wu, X.; Zhang, Z.; Yu, J.; Qiu, H.; Hong, J. H.; Jin, C. H.; Li, J. X.; Wang, X. R.; et al. Top-down Fabrication of Sub-Nanometre Semiconducting Nanoribbons Derived from Molybdenum Disulfide Sheets. *Nat. Commun.* **2013**, *4*, 1776.
(57) Nozaki, J.; Fukumura, M.; Aoki, T.; Maniwa, Y.; Yomogida, Y.; Yanagi, K. Manipulation of Local Optical Properties and Structures in Molybdenum-Disulfide Monolayers Using Electric Field-Assisted near-Field Techniques. *Sci. Rep.* **2017**, *7*, 46004.
(58) Ryu, Y.; Kim, W.; Koo, S.; Kang, H.; Watanabe, K.; Taniguchi, T.; Ryu, S. Interface-Confined Doubly Anisotropic Oxidation of Two-Dimensional MoS_2. *Nano Lett.* **2017**, *17*, 7267−7273.
(59) Das, S. R.; Wakabayashi, K.; Yamamoto, M.; Tsukagoshi, K.; Dutta, S. Layer-by-Layer Oxidation Induced Electronic Properties in Transition-Metal Dichalcogenides. *J. Phys. Chem. C* **2018**, *122*, 17001−17007.
(60) Singh, A. K.; Zhou, L.; Shinde, A.; Suram, S. K.; Montoya, J. H.; Winston, D.; Gregoire, J. M.; Persson, K. A. Electrochemical Stability of Metastable Materials. *Chem. Mater.* **2017**, *29*, 10159−10167.
(61) Yin, M.; Li, Z.; Kou, J.; Zou, Z. Mechanism Investigation of Visible Light-Induced Degradation in a Heterogeneous TiO_2/Eosin Y/Rhodamine B System. *Environ. Sci. Technol.* **2009**, *43*, 8361−8366.
(62) Gao, J.; Li, B.; Tan, J.; Chow, P.; Lu, T.-M.; Koratkar, N. Aging of Transition Metal Dichalcogenide Monolayers. *ACS Nano* **2016**, *10*, 2628−2635.

DOI: 10.1021/acsomega.9b01067
ACS Omega 2019, 4, 10322−10327